Research Square

Preprints are preliminary reports that have not undergone peer review.
They should not be considered conclusive, used to inform clinical practice,
or referenced by the media as validated information.

Intracortical recordings in human lateral occipital complex support the biased- competition model of spatial attention

Michaël Vanhoyland

michael.vanhoyland@kuleuven.be

KU Leuven and the Leuven Brain Institute

Jesus Garcia Ramirez

KU Leuven and the Leuven Brain Institute

Peter Janssen

KU Leuven and the Leuven Brain Institute

Tom Theys

KU Leuven and the Leuven Brain Institute

Article

Keywords:

Posted Date: May 29th, 2026

DOI: https://doi.org/10.21203/rs.3.rs-9718483/v1

License: This work is licensed under a Creative Commons Attribution 4.0 International License.
Read Full License

Additional Declarations: No competing interests reported.

Abstract

Spatial attention is fundamental for prioritizing relevant information in complex visual environments. Yet, the neural mechanisms underlying this process in humans remain elusive given the spatiotemporal constraints of functional imaging. Here we present multi-unit spiking activity from the human lateral occipital complex (LO) during a covert spatial visual attention task. Spatial attention strongly modulates neural activity when multiple competing stimuli are present in the receptive field, but not when one stimulus is outside the receptive field, supporting the biased-competition model of attention. This model suggests that spatial attention reduces interference between stimuli by favoring the attended one. Additionally, we found that attention and keeping an object in working memory extends the neural representation of an object. Crucially, our study offers the first demonstration of the neural effects of spatial attention in human visual cortex and a more naturalistic insight into human visual attention, as the participants received no prior training, unlike electrophysiology studies on trained macaques. Our study bridges human neuroimaging and primate electrophysiology, providing unique insights into the neural basis of attention.

Introduction

The human visual system is constantly bombarded with an overwhelming amount of information, yet it cannot process all elements equally. Selective attention prioritizes relevant stimuli for enhanced neural processing, thereby guiding behavior efficiently. Seminal studies, such as Posner's spatial orientation paradigm[1] and Treisman's feature-integration theory[2], established that spatial attention filters irrelevant distractors, reducing cognitive load and boosting performance in tasks like visual search and object recognition.

Animal models, particularly macaque monkeys, have been used to study the neural basis of spatial attention. Spatial attention modulates activity across striate and extrastriate cortices in the dorsal and ventral visual pathway[3–12]. When attention is directed to a stimulus in a neuron's receptive field (RF), responses are enhanced, manifested as increased firing rates (equivalent to higher effective contrast), strengthened gamma-band synchronization, and reduced response variability and noise correlations[3,4,7,13–17]. While stimuli presented outside the RF do not elicit a neural response, they could still modulate the neural response of stimuli presented within the RF[18,19]. These modulatory effects are themselves modulated by spatial attention: directing attention to a stimulus outside the RF increases its inhibitory effect on the neural response to a stimulus presented within the RF, while directing attention to a stimulus within the RF decreases the inhibitory effect of distractors presented outside the RF[5].

These observations align with the biased competition model of attention[20], which posits that attention resolves competition among stimuli within a neuron's receptive field by biasing the neural population's representation towards the attended stimulus, effectively simulating its presentation in isolation. Supporting this, electrophysiological recordings in monkeys' inferotemporal cortex have shown that attention in cluttered displays restores population-level representations of attended objects to patterns

resembling their isolated presentation, enabling linear decoders to accurately identify the object only under attended conditions[10].

Extrapolating these insights to humans presents challenges: animal studies often rely on extensively trained subjects, potentially introducing task-specific strategies that limit generalizability[21]. In humans, fMRI and event-related potentials studies have revealed similar effects, with enhanced activation in visual cortex contralateral to attended locations[22,23]. A landmark fMRI study demonstrated mutual suppression among simultaneously presented competing stimuli in the absence of attention, which was partially alleviated by directed spatial attention, consistent with biased competition[24]. However, noninvasive methods remain an indirect measurement of neural activity and are limited in spatiotemporal resolution.

To overcome the aforementioned limitations, we performed intracortical recordings from three multi-electrode arrays in two neurosurgical patients in the lateral occipital complex (LO), a key region for object recognition[25–28]. By employing a covert spatial visual attention task, we directly measured neural activity in humans in the absence of extensive training. In this task, patients were required to press a button when they detected a specific object at a specific location.

Our results show that attentional effects are significantly enhanced when multiple stimuli compete within the receptive field, resulting in a greater number of attention-modulated sites and significant decoding accuracy for identifying the attended location. Furthermore, our decoding analysis supports the biased-competition model of attention. Notably, we find that attention selectively extends the neural representation of an object within its receptive field. Overall, our results offer a high-resolution view of the neural mechanisms supporting the prioritization of behaviorally relevant stimuli via spatial attention, shedding new light on this critical cognitive process.

Results

We recorded multi-unit activity from 3 micro-electrode arrays (A1-3) implanted in LO of 2 patients (P1 and P2). All arrays responded stronger to non-scrambled images compared to scrambled images of objects, compatible with expected responses for LO, as shown in previous research.[29] Exact anatomical locations of the arrays are presented in Fig. 1A. Patients performed a cued covert visual attention task in which two images were shown simultaneously left and right of the fixation marker. Patients were instructed to press a button upon detecting a target object at one of both possible presentation locations (Fig. 1B). P1 could make a response from the moment of stimulus onset, whereas a fixed delay period was enforced after stimulus presentation for P2, in order to investigate sustained responses despite discontinued stimulus presentation. Both patients performed near-perfect, despite P1 requiring a brief learning period (Fig. 2). Subsequent analyses focus exclusively on correct trials.

(A) Anatomical locations of Utah arrays projected on a common MNI template of the brain. MNI coordinates (X, Y, Z) are as follows: A1 (-35, -89, -8), A2 (-41, -83, 9) and A3 (-38, -84, -5). Blue arrays

represent competition arrays, red represents non-competition array. Array 2 and 3 were implanted in the same patient (P2). Adapted from Bougou, V., Vanhoyland, M., Bertrand, A. et al. Neuronal tuning and population representations of shape and category in human visual cortex. Nat Commun 15, 4608 (2024).[30] **(B)** Schematic of the spatial attention tasks. Patients were instructed to press a button if they witnessed the cued object in the correct location. Above, scheme for P1: Trials began with central fixation (200–300 ms), followed by the simultaneous presentation of two object images. A verbal cue at the start of each block indicated the target object and the side of the screen where the target would trigger a button press response. After stimulus presentation (300 ms), the patient responded via button press. Below, scheme for P2: A visual cue (3000 ms) at block start indicated the target object and location. Trials involved central fixation (200–300 ms), followed by two object images (500 ms). After a blank screen delay (700 ms), the fixation marker changed color, signaling the response period. **(C) Left**. Electrode array configurations with respect to stimulus presentation. In competition arrays (A1 and A2, blue) the average RF encompassing both object presentation locations. In contrast, only the right location was within the average RF of the no-competition array (A3, red). **Right.** Heatmap showing the population average RF per recorded array. Overlayed dashed boxes correspond to both objects' presentation locations.

(A) Proportion of correct responses (Hit Rate, blue bars) and correct rejections (Correct Rejection Rate, orange bars) for each cue condition for P1 (Left) and P2 (Right). Hit Rate refers to the proportion of trials where the patient correctly responded to the cued target. Correct Rejection Rate refers to the proportion of trials where the patient withheld a response when no target was present. **(B)** Box plots showing the reaction times (ms) for correct detections across cue conditions for P1 (Left) and P2 (Right). Box plots indicate median (middle line), 25th, 75th percentile (box), and box limits ± 1.5 × interquartile range (whiskers).

Visual responsiveness and receptive field mapping

We recorded activity from 146 visually responsive multiunits (MUAs) (N_{A1} = 64, N_{A2} = 30, N_{A3} = 52). The multi-electrode recoding design and time constraints that accompany invasive neural recordings in human subjects make it impossible to adjust the stimulus location based on the receptive field of each individual neuron separately. Therefore, we first determined the average RF per array (Fig. 1C). Stimulus positions were then chosen so they fell within the average RF of A1 in P1 and A2 in P2. Since the positions were not tailored to the response properties of A3 in P2, and A3 showed a more heterogeneous pattern with both foveal and contralateral responses, only the right location was within the average RF of A3. As a result, the 2 concurrently presented objects competed for neural representation in A1 and A2 ('competition arrays'), but not in A3 ('non-competition array') (Fig. 1C). To make substantiated claims about attentional effects when decoding stimulus identity or position, it is essential that stimuli evoke similar responses across the RF. We therefore performed a control task in P2 where objects were presented in both locations separately, while patients were inattentive to the objects (Fig. 3). Example single units of A2 and A3 (derived after spike sorting the MUA sites) are presented in Fig. 3B. The unit

from A2 responded equally to objects at both locations, whereas the A3 unit responded only to the contralateral location. This pattern confirms that both objects were inside the RF of the A2 unit, while only one was inside the RF of the A3 unit. To quantify these effects at the population level, we used time-resolved Kolmogorov-Smirnov (KS) distance analysis (Fig. 3C) that measures the separation between firing rate distributions under different conditions (objects presented on one side vs. the other). This confirmed a clear separation of response distributions in A3 - consistent with being a non-competition array - with a less pronounced separation for A2.

(A) Schematic of the attention control task that was performed in array 2 and 3. The patient had to press a button if she noticed a change in the color of the fixation marker. Each trial began with central fixation (200–300 ms), followed by the presentation of an individual object from the attention task stimulus set at one of both task locations. After stimulus presentation (300 ms), the patient responded via button press. **(B)** Example single units per array. Average net spike rate for trials where the object was presented at the ipsilateral location (left, blue) and contralateral location (right, red). Horizontal black lines indicate time windows with statistically significant differences between left and right trials (two-sided independent samples t-test, $p < 0.01$). At the right side of each graph, the waveform and receptive field is presented (time window 100–250 and 200–350 ms after stimulus onset was used for array 2 and 3, respectively). **(C)** Kolmogorov-Smirnov (KS) distances across time. Each row illustrates the KS distance of a visually responsive site between distribution of trials with objects presented at the left versus trials with objects presented to the right. Time bins are shown on the x-axis and values represent the middle of a 100 ms bin. Sites are sorted in ascending order from top to bottom according to the maximum KS distance.

Neural coding of locus of attention

We first examined whether directing attention to the left or right stimulus during simultaneous bilateral presentation modulated neural activity. Example MUAs from each array are shown in Fig. 4A. In the competition arrays, neural responses were strongly modulated by the attended side, whereas no such modulation was observed in the non-competition array. Importantly, each stimulus appeared equally often on both sides, ruling out stimulus-frequency confounds. To quantify effects at the population level, we again employed time-resolved KS distance analysis to compute the difference in the response distribution between stimuli attended to the left or right (Fig. 4B). A significant proportion of sites in the competition arrays exhibited locus of attention selectivity (42% for A1 and 37% for A2, two-sided permutation test, $p < 0.01$). Moreover, the proportion of attention-selective sites in the no-competition array (10% for A3, two-sided permutation test $p < 0.01$) was significantly lower than in both competition arrays ($p = 9.48 \times 10^{-5}$, $p = 2.9 \times 10^{-3}$, z-test for two proportions for A1 and A2, respectively).

To better evaluate the amount of information that is stored in the neural population about the attended locus, we trained linear decoders to classify the attended side based on the responses to one object, and tested if the decoder's predictions about locus of attention would generalize to other attended objects

(Fig. 5A). By using different objects in training and testing set, we isolated the effect of locus while simultaneously mitigating the risk of decoder overfitting and attention bias towards one object. The attended location was readily decodable from both competition arrays, peaking around 180 ms after stimulus onset (two-sided permutation tests, $p < 0.005$). A2 exhibited sustained high decoding accuracy throughout the stimulus and delay periods, while decoding accuracy declined rapidly after stimulus offset in A1. Importantly, P1 (A1) was not instructed to maintain the decision in working memory after stimulus offset, contrary to P2. Decoding accuracy for the cued location in the non-competition array A3 was not significant (Fig. 5B). Overall, these results suggest that - in case two stimuli are presented within the receptive field - spatial attention modulates neural activity.

(A) Average net spike rate for trials attending left (blue) and right (red) across example sites from each recording array. Horizontal black lines indicate time windows with statistically significant differences between left and right trials (two-sided independent samples t-test, $p < 0.05$). **(B)** Kolmogorov-Smirnov (KS) distances across time. Each row illustrates the KS distance of a visually responsive site between distribution of trials attending to the left versus trials attending to the right. Time bins are shown on the x-axis and values represent the middle of a 100 ms bin. Sites are sorted in ascending order from top to bottom according to the maximum KS distance.

To evaluate if the neural code was stationary over time, we investigated if the decoder would generalize across time bins in both competition arrays. If different neurons are recruited over time in a predictable and constant order (reflecting a non-stationary code), this would result in significant decoding over time, without cross-temporal decoding generalization since the neural code is composed of different neurons over time. Results for cross-temporal decoding analysis are shown in Fig. 5C. Diagonal decoding accuracies reflect performance at identical time bins (as in Fig. 5B). In the training analysis, both training and testing were done on the same object (same as blue curves in Fig. 5B), whereas another object was used for testing in the generalization analysis (same as red curves in Fig. 5B). The results indicate a stationary neural code during stimulus presentation for both arrays as we observed strong cross-temporal generalization during stimulus presentation. Generalization was only maintained after stimulus offset in the presence of a delay as seen in A2, but not in A1.

(A) Schematic of the cross-condition generalization procedure for decoding the locus of spatial attention. Linear decoders were trained to discriminate between trials attending to left (ipsilateral, yellow) versus right (contralateral, green) using one target object (Keyboard and Hands for P1 and P2, respectively) and tested on generalization data of trials with the other target object (Guitar and Legs for P1 and P2, respectively). **(B)** Time course of decoder performance (Accuracy) for predicting the locus of attention regardless of the stimulus in the competition (A1 and A2, green) and no competition (A3, blue) conditions. Lines and shading show mean ± standard error classification accuracy for (blue) decoders trained to discriminate between the attended locations using trials with one target object and tested using held-out data from the same target object. Red curves correspond to cross-condition generalization performance, where the decoder is tested using data from a different target object. Distribution reflects 10-fold grouped cross-validation. Horizontal bars indicate above-chance

classification ($p < 0.005$; one-sided permutation test with at least five consecutive significant time points). **(C)** Temporal dynamics of spatial attention effects. Cross-time decoding analysis for competition arrays (A1 and A2) for trials with the training target object (same as in Fig. 5B) and for the trials for the generalization object. Color scale represents decoding accuracies for linear decoders trained to predict the locus of attention. Training time of the decoder is shown on the y-axis and test time is shown on the x-axis. Dashed blue lines represent times of stimulus onset and offset. Note the drop in accuracy after the second blue-dashed line in the generalization analysis of A1. In **(B-D)**, time bins on x-axis **(B-C)** and x- and y-axis **(D)** represent the middle of a 150 ms bin used for decoding.

Effect of spatial attention on object representations.

To assess how attention influences object representations under conditions with and without receptive-field competition, we trained linear decoders in two ways: (1) to predict the stimulus at the attended location (Fig. 6B), and (2) to predict the stimulus at a fixed spatial location irrespective of the current locus of attention (Fig. 6C). In both analyses, decoders were trained on trials in which attention was directed to one location and tested on trials in which attention was directed to the opposite location. Thus, the same test data were used in both cases, but with different predictive goals: in (1) the decoder attempted to identify the stimulus at the opposite attended location, whereas in (2) it attempted to identify the stimulus at the originally cued (now unattended) location. Training and testing the decoder on the same attended location allowed us to estimate the maximum visual information available in the neural population. Predicting the stimulus at the opposite attended location provided a measure of attentional dependence. Successful generalization across attended locations would indicate that spatial attention stabilized the neural representations. Conversely, successful decoding of stimuli at the unattended location would suggest that object information is represented in a manner that is relatively independent of attentional modulation.

All arrays encoded significant information about the attended stimulus (one-sided permutation test, $p < 0.005$, blue curves, Fig. 6B). While decoding time courses differed between arrays in their onset (around 100 ms for A1, 200 ms for both A2 and A3), peak performance converged around 400 ms post-stimulus onset. Importantly, this robust decoding generalized across attended locations when both objects were presented in the RFs (one-sided permutation tests, $p < 0.005$, red curves, Fig. 6B, competition arrays A1 and A2), but not when only one object was inside the receptive field (non-competition array A3). When decoding a target object irrespective of the locus of attention, there was significant generalization of decoding in the non-competition array (one-sided permutation test, $p < 0.005$, Fig. 6C), but no generalization was observed in both competition arrays. Taken together, these results suggest that when multiple stimuli fall within the RF, the neural code selectively represents the attended stimulus (e.g. hand). In contrast, when only a single object is present within the receptive field (as on the right side for A3), the neural code reflects that stimulus regardless of whether it is attended.

Next, we again investigated if the decoders would generalize across time. For this we trained the decoder on the contralaterally (right) attended objects and predicted 1) contralaterally attended objects,

2) ipsilaterally attended objects and 3) contralaterally unattended objects. Results for cross-temporal generalization are presented in Fig. 6D. In all arrays, decoding of an attended contralateral object within the receptive field was stable, persisting into the delay period (center matrices in Fig. 6D). Similarly, the decoding generalized to ipsilaterally attended objects, but only if they were presented within the RF (competition arrays A1 and A2, left matrices in Fig. 6D). In contrast, an unattended object in the RF was only decodable if it was the only object present in the RF (non-competition array A3, right matrices in Fig. 6D). Collectively, these findings suggest that attention and maintenance of an object within working memory selectively prolongs the neural representation of an object when presented in the receptive field.

(A) Schematic of the procedure for decoding the object at the attended location (above) and fixed location (below). In both procedures, the decoder was first trained on trials attending to the right (blue square) to predict the attended object at the right (blue circle) and then tested for generalization on trials where attention was directed to the other location (red square). The red circle shows where an object was predicted during testing for generalization. Therefore, the generalization for attended location analysis investigated if an object was decodable at an attended location while being trained at another, but also attended, location. The generalization for fixed location analysis investigated if an object was decodable at an unattended location while being trained at the same, but attended, location. **(B)** Time course of decoder performance (accuracy) for each recording session. Lines and shading show mean ± 1std classification accuracy for (blue) decoders trained to decode the object at the attended location when the decoder is trained and tested at the same location and (red) decoders trained at one location and tested on the other. Distribution reflects 10-fold grouped cross-validation. Horizontal bars indicate above-chance classification ($p < 0.005$; one-sided permutation test with at least five consecutive significant time points). **(C)** Time course of decoder performance for each recording session. Lines and shading show mean ± 1std classification accuracy for (Blue) decoders trained to decode the object at a fixed location when the decoder is trained and tested at the same location and (Red) decoders trained at one fixed location and tested on the other. Distribution reflects 10-fold grouped cross-validation. Horizontal bars indicate above-chance classification ($p < 0.005$; one-sided permutation test with at least five consecutive significant time points). **(D)** Cross-time decoding analysis for neural decoders trained to predict the stimulus at different locations for every recorded array (upper plots are competition arrays, lower plots are from the non-competition array). For each array, central matrices present cross-time decoding analysis for the training case, where decoders were trained to predict the stimulus located at the right when attention is directed to the right. In contrast, the left and right matrices display cross-time decoding performance in the generalization cases, where the training decoder is tested to predict the stimulus at either the right or left locations when attention was directed to the left. Decoding accuracies for linear decoders trained on attended locations are color-coded. Training time is plotted on the y-axis, and test time on the x-axis. Dashed blue lines indicate stimulus onset and offset. In **(B, C and D)**, time bins on x-axis (**B,C**) and x- and y-axis (**D**) represent the middle of a 150 ms bin used for decoding.

Discussion

In this study, we present, to our knowledge, the first direct recordings from human LO during a covert spatial visual attention task, revealing that spatial attention dynamically modulates neural activity in LO. Our findings reveal that attentional effects are significantly enhanced when multiple stimuli compete within the RF, leading to a greater number of attention-modulated sites, significant decoding accuracy for identifying the attended location, and stable temporal dynamics of the population code for spatial attention throughout stimulus presentation. Notably, our decoding analysis presents supporting evidence for the biased-competition model of attention, which posits that spatial attention reduces the interference between multiple stimuli by favoring the relevant one.

We observed a higher number of sites modulated by the attended location and superior decoding performance for the locus of attention in competition arrays, compared to the non-competition array where only a single stimulus is present inside the RF. These findings are consistent with previous electrophysiological studies in non-human primates[17], which have demonstrated that spatial attention exerts a more pronounced influence when multiple stimuli compete for representation within the RF.

Notably, our results diverge from reports showing enhanced firing rates to single stimuli inside the RF when attended[6,13,17,31–34]. In our study, we unexpectedly found no significant decoding for the locus of attention in the non-competition array across all time periods. Moreover, decoders trained on attended stimuli within the RF unexpectedly generalized fully for unattended stimuli within the RF for the first 400 ms (with only a small drop in decoding accuracy after 400 ms) if only a single stimulus was presented within the RF. It has been shown in macaque V4 that directing attention to the RF surround, or even distant locations, reduces spike rate for the stimulus presented within the RF[5]. Therefore partial decoder generalization was expected. One possible explanation for these discrepancies lies in the high-contrast stimuli employed in our study. According to the normalization model of attention[35], attention-driven increases in firing rates are proportional to the contrast of the attended stimulus, saturating above a certain level of contrast. This suggests that the high-contrast stimuli used in our study may have masked any potential attentional modulation, leading to the absence of significant decoding for the locus of attention in the non-competition array.

Our analysis revealed a stationary neural code for attended locations during stimulus presentation, consistent across training and generalization conditions for both arrays with competing stimuli inside the RFs. This stability suggests a robust representation of attended locations in extrastriate visual cortex, enabling efficient processing of relevant sensory information[15,36]. Notably, we observed distinct differences in the post-stimulus phase of the response between patients, which can be attributed to the differing task demands. In P1, where responses could be made immediately after stimulus onset, decoding accuracy diminished after stimulus offset. This suggests that information about the attended location was not maintained beyond stimulus presentation, as there was no requirement to hold this information in working memory. Instead, attentional resources were rapidly reallocated after stimulus processing, allowing for efficient switching between tasks. In contrast, the task paradigm for P2 introduced a delay period before response execution, necessitating active maintenance of attended

location information. Consistent with this demand, spatial attention was sustained throughout the delay period in A2 (competition array). This finding is in line with previous studies showing that delayed responses require the engagement of working memory systems to maintain task-relevant information[37,38]. By dissociating these two conditions, our findings demonstrate that the neural representation of spatial attention is dynamically adjusted based on task demands. Specifically, when immediate responses are possible, attentional resources are rapidly reallocated after stimulus processing, whereas attentional information is actively maintained to ensure accurate performance when delayed responses are required.

We demonstrated that attention selectively extends the neural representation of an object in the RF, which could reflect prioritization for further processing. This phenomenon might be crucial for behaviors that require detailed information about the object, such as visually searching for a specific item[39]. The sustained neural representation of attended objects has significant implications for understanding how attention influences visual perception and memory. For instance, selective attention may facilitate the consolidation of stimuli into working memory, enabling their maintenance over longer periods[40]. This is consistent with theories suggesting that attention plays a key role in gating information into working memory[36,37]. Notably, our findings have broader implications for understanding how attention shapes neural processing and behavior. The selective prolongation of neural representations may enable more efficient information processing and retrieval, ultimately influencing performance in tasks that require attention and memory[41].

The functional properties of cortical neurons are not fixed. Instead, responses can vary based on the behavioral context via top-down processes. Spatial attention is one of the most studied top-down processes in the literature. Our findings underscore the impact of higher-order cognitive processes on early visual processing. Importantly, while neural responses for objects were modulated by selectively directing attention to different locations the RF, neural responses in LO are invariant for positional shifts within the receptive field when stimuli are presented across the RF without directed attention[42]. Enhanced attentional effects when multiple stimuli compete within the RF, and the sustained representation of attended objects, indicate however that top-down signals influence visual processing.

Since similar effects in macaque visual cortex have been reported, our study represents a crucial validation of numerous previous studies on spatial attention. However, macaque studies often involve highly trained animals, possibly optimizing their responses to specific stimuli or tasks[43–45]. Importantly, the human subjects in our study did not undergo any prior training, avoiding task-specific optimization and offering a more naturalistic view of attentional processes in the human visual system. Furthermore, most macaque studies have selected neurons based on their responses and isolation characteristics (spike amplitude) which may induce a recording bias, whereas the use of micro-electrode arrays in our study prevented such bias.

Our study provides unprecedented spatial and temporal resolution data that serves a critical foundation for understanding spatial attention in humans, but several key questions remain to be addressed. A

crucial next step will be to elucidate the neural mechanisms underlying the sustained representation of attended objects, including the specific circuits and processes involved in prolonging neural responses to visual stimuli. Furthermore, exploring how spatial attention operates in diverse task contexts will be essential for developing a comprehensive understanding of its role in cognition and brain function.

Materials and Methods

Study approval

We obtained ethical approval (study number s53126) for conducting semi-chronic microelectrode recordings using the Utah array in patients undergoing invasive epilepsy monitoring. The study protocol was approved by the local ethical committee (Ethische Commissie Onderzoek UZ/KU Leuven). The study was carried out in accordance with the principles of the Declaration of Helsinki, the principles of good clinical practice, and all applicable regulatory requirements set by the Federal Agency for Medicines and Health Products (FAGG).

To ensure safety and compliance, strict adherence to imposed safety measures was maintained. This included the use of case report forms and detailed reports on any (serious) adverse events. All data collected during the study were encrypted and stored at the University Hospitals Leuven. The study was thoroughly discussed with the patients during the pre-operative consultation, which took place at least six weeks before the surgery. The patients were informed about the risks associated with micro-electrode array implantation, such as infection and hemorrhage. No additional incisions were made for the purpose of this study. Written informed consent was obtained from the patients on the evening prior to their surgery.

Clinical information

We obtained invasive intracranial recordings from the lateral occipital cortex in 2 refractory epilepsy patients. Patient 1 was a 55-year old female with neurofibromatosis type 1 (NF1). She suffered from a left occipito-temporal brain hemorrhage caused by venous sinus thrombosis at the age of 35 (MNI coordinates: anterior border (-65,-45, -5), superior border (-54,-62,6), posterior border (-53,-75,-2) and inferior border (-54,-60,-16)). She had no intracranial tumors. Patient 2 was a 58-year old female suffering from recurrent psychotic episodes. Patient 1 was implanted with one array, while two arrays were implanted in patient 2.

Both patients were taking chronic anti-seizure medications: patient 1 was on Levetiracetam 2000 mg and Lamotrigine 225 mg, both twice daily. Patient 2 was on Levetiracetam 2000 mg, Diphantoine 100 mg, Clonazepam 1 mg and Lacosamide 300 mg, all twice daily. During admission to the epilepsy ward, the anti-seizure medications were adjusted for both patients based on the number of detected seizures.

Utah arrays were located adjacent to the clinical macroelectrodes, consistent with previous studies using micro-electrode arrays[27,29,30,46–50]. Target locations of intracranial electrodes were determined by

the epileptologist in a multidisciplinary consensus meeting and were based on electroclinical findings and non-invasive multimodal imaging. Multi-electrode arrays were implanted via the craniotomy performed for the implantation of subdural grids, adjacent to the grids. The arrays were removed during the same surgery for subdural grid removal, 14–16 days after implantation. Both insertion and removal of electrodes were done under general anesthesia. No new neurological deficits, nor implantation-related complications (infection, hemorrhage, wound problems) were recorded.

Although the presumed epileptogenic onset zone encompassed the lateral occipital cortex based on multimodal preoperative assessment, the arrays were inserted outside the presumed epileptogenic onset zone in both patients. In patient 1, invasive recordings showed no clear focal onset. In patient 2, seizure onset was multifocal and no resection was proposed. In both patients, multi-unit spiking activity was analyzed to investigate to what extent neural activity could predict seizure onset[51].

Imaging

We acquired a T1-weighted image using a 3-T MR scanner (Achieva dstream, Philips Medical Systems, Best, the Netherlands) at the University Hospitals Leuven for presurgical planning and to reconstruct the postoperative electrode location. The imaging parameters were as follows: echo time of 3.1 ms, inversion time 900 ms, slice thickness 1.0 mm, 400 × 400 matrix, and 283 coronal slices. Following electrode placement, a CT scan (Siemens) was performed with a slice thickness of 1 mm, a voltage of 120 kV, and a dose length product of 819 mGy.cm. The CT scan served to verify the electrode locations and to rule out any hemorrhage.

For imaging preprocessing, we utilized SPM12 software (Wellcome Department of Cognitive Neurology, London, UK) running on MATLAB (Mathworks, Natick, MA). The preprocessing steps included (1) Setting the anterior commissure as the origin for both the MRI and CT scan (2) Realigning the images (3) Coregistering the MRI and CT images and (4) Warping the MRI and coregistered CT to a common high-resolution brain atlas (MNI 152)[52]. To generate cortical 3D renderings of the subjects' pial surfaces and the high-resolution MNI atlas, we employed Freesurfer. The precise electrode location on the cortical surface and the MNI coordinates were determined using iElectrodes Software[53].

Invasive recordings

We recorded from 96-electrode arrays (Utah ArrayTM – Blackrock Neurotech) from day 1 until day 14 after array implantation. We inserted the array using a pneumatic inserter wand provided by Blackrock Neurotech. We closed the dura above the array and placed the bone flap on top to secure the array. We placed reference wires subdurally and ground wires epidurally. We digitally amplified the signal using a Cereplex M head stage, connected to a 128-channel neural signal processor (Blackrock Neurotech), and sampled the signal using Central Software at a sampling rate of 30 kHz. We applied a 750 Hz high-pass filter for spiking activity. We set the multiunit detection threshold at 3 standard deviations below the

noise band. We considered units recorded on the same electrode but on different days as separate units. The variable signal quality in the immediate postoperative period resulted in a difference in the number of responsive and selective sites during each recording session. All spike sorting was performed offline (Offline Sorter 4, Plexon, TX).

Stimulus presentation

We conducted experiments in a dimmed hospital room. We utilized custom-built software to present stimuli on a 60 Hz DELL-P2418HZM LED monitor. Patients sat 60 cm away from the screen (1 pixel = 0.026 deg). We instructed them to focus on a small red square (0.2 × 0.2°) positioned at the center of the display. We continuously monitored the position of their left or right pupil using a dedicated eye tracker (Eyelink 1000 Plus, 1000 Hz) in head free-to-move mode. If they deviated from the electronically defined 3° by 3° fixation window, the trial was aborted. To synchronize the data, we attached a photodiode to the upper left corner of the screen, which detected a bright flash coinciding with the first frame of the stimulus. This flash was invisible to the patients. To accurately record baseline spike rate activity, we introduced an intertrial interval between the offset of the stimulus and the onset of fixation for the next trial.

Spatial attention task(s)

In this task (Fig. 1B), we investigated the effects of covert spatial attention by presenting two images of objects simultaneously and instructing the subjects to signal the presence of a specific target object in a designated location with a button press (e.g., ‘press the button if you see a hand on the right’)

P1 received a verbal cue at the start of each block indicating the target object and the side of the screen where the target image would appear. Trials involved the simultaneous presentation of two object images, each depicting a musical instrument, on either side of a central fixation point. Individual trials within a block followed this sequence: The patient fixated a central marker for a random duration (200–300 ms, uniform distribution), followed by the presentation of two object images for 300 ms. The patient could respond from the moment of stimulus onset until the end of the intertrial interval, which lasted 300ms before the start of the next trial. Trials within a block were presented in a pseudorandomized order until the patient correctly responded to 10 trials for each of the 24 possible stimuli.

P2 performed a similar task but with a visual cue instead of a verbal one. Trials were also structured in blocks, each beginning with a 3000 ms cue presentation indicating the relevant location for the upcoming trials. Individual trials within a block followed this sequence: The patient fixated a central marker for a random duration (200–300 ms, uniform distribution), followed by the presentation of two object images (hands or legs) for 500 ms. A blank screen was then presented for a fixed delay of 700 ms, after which the color of the fixation marker changed to signal the patient's response period. Finally, a 300 ms intertrial interval preceded the start of the next trial. Trials within a block were presented in a pseudorandomized order until the patient correctly responded to one trial for each of the 18 possible stimuli.

Control task

We recorded an additional control task for P2 before the attention task in the same session (Fig. 3A). In this task, we instructed the patient to press a button if the fixation marker changed color. Trials involved the presentation of one object image from the individual objects used to create the attention task stimulus set, on either side of a central fixation point. Individual trials followed this sequence: The patient fixated a central marker for a random duration (200–300 ms, uniform distribution), followed by the presentation of one object for 250 ms. The patient could respond from the moment of stimulus onset until the end of the intertrial interval, which lasted 300ms before the start of the next trial. Trials were presented in a pseudorandomized order until each of the 12 possible stimuli was correctly shown 10 times.

Stimulus and Target Properties

Stimuli for both patients consisted of pairs of achromatic images presented on a uniform background. Each patient was shown a different set of images evoking strong neuronal responses. For P1, stimuli depicted musical instruments on a random noise black and white background, derived from the study of Bracci et al [54]. We used all possible combinations of individual instrument images to ensure a balanced spatial distribution, excluding pairings of identical instruments. Images subtended a mean visual angle of 2° vertically and 2° horizontally. For P2, stimuli depicted images of hands and legs on a white background. Images were grouped into two categories (hands and legs), and we ensured that two images from the same category were never presented together to control for potential biases. Images for P2 subtended a mean visual angle of 7° vertically and 3.5° horizontally.

Within each block, trials were designated as either "target trials" (requiring a button press response) or non-target trials. The proportion of target trials was 12.5% for P1 and 50% for P2.

Receptive Field measurement

To characterize the receptive field (RF) properties of the recorded neural populations, we conducted an RF mapping task prior to the main spatial attention task. This task was performed while patients maintained central fixation. To ensure fixation compliance, patients were instructed to press a button with their right hand whenever a visual distractor (red or green cross) appeared at the fixation point in a small percentage of trials (~ 2%).

The specific stimuli used for RF mapping were tailored to the recorded neural populations, accommodating differences in selectivity and RF size across arrays.

Patient P1: A single monochromatic face image (2° by 2°) from the Popivanov et al. study [55] was selected based on its ability to evoke strong responses across multiple recording sites. This image was presented at 100 non-overlapping locations, covering a 20° by 20° region of the central visual field. Stimuli were presented for 400 ms following a 300 ms fixation period, with a 50 ms intertrial interval. Each image was repeated 7–10 times.

Patient P2: Due to time constraints, we mapped the RFs of arrays 1 and 2 in P2 simultaneously. A single monochromatic human body image (4° by 4°) from the same study was chosen for its strong activation of the recorded sites. This image was presented at 49 locations, covering a 28° by 28° region of the visual field. Stimulus presentation was 300 ms, with a 250 ms fixation period and a 150 ms intertrial interval. Each image was repeated 7–10 times.

Preprocessing – Removing unstable channels

To avoid potential confounds in our blocked experimental design, we excluded any channels that did not exhibit stable recordings throughout a session. Stability was assessed by dividing the baseline rates for every trial into equal-sized blocks of 10 trials, measuring the average firing rate of each neuron within each block. We then performed two statistical tests: the Augmented Dickey-Fuller (ADF) test to evaluate the presence of a unit root in the time series of block-averaged firing rates, and the Kwiatkowski-Phillips-Schmidt-Shin (KPSS) test to examine the null hypothesis of stationarity. A significant result ($p < 0.01$) in the ADF or in the KPSS test indicates non-stationarity, suggesting that the channel's firing characteristics changed over the session. Channels exhibiting non-stationarity according to either test were classified as unstable and removed prior to subsequent analysis. This procedure resulted in the exclusion of 31 channels from array A1, 8 channels from A2, and 10 channels from A3.

Single-site data analysis

We computed multi-unit firing rates for each correct trial in two analysis windows: a baseline window ranging from 250 before stimulus onset to stimulus onset and a response window ranging from 150 to 400 ms after stimulus onset. We restricted all analyses to visually responsive sites. To assess the responsiveness of each recorded site, we performed one-sided dependent samples t-tests between the spike rates in the baseline and response windows for each attention condition separately (e.g. baseline vs looking for a hand at the right side). For every experiment separately, we considered a site as visually responsive if any of these comparisons was significant ($p < 0.01$). All subsequent analyses were based on the baseline subtracted, average net firing rates. In cases where responses across sites were shown on the same figure, we normalized the average net firing rates for each site in the range $(x_{min} = 0,\ x_{max} = 1)$ as follows:

$$r\left(i\right)\ = \frac{r\left(i\right) - \ r_{min}}{r_{max} - r_{min}}$$

In which, $r\left(i\right)$ corresponds to the average net response for stimulus i for that site r_{max} and r_{min} correspond to the “best” and “worst” stimuli for that site, respectively.

Kolmogorov-Smirnov distance

To assess the influence of spatial attention on neural responses, we employed the Kolmogorov-Smirnov (KS) distance for each recorded site. Firing rates were computed within 100 ms bins using a 10 ms sliding window, facilitating a time-resolved analysis of attentional modulation. For each time bin, we calculated the KS distance by determining the maximum vertical distance between the cumulative

distribution functions (CDFs) of firing rates under two attention conditions: trials where the patient attended to the left versus trials where they attended to the right.

The KS distance is a normalized measure of the separation between the two firing rate distributions obtained when the patient was attending to one side versus to the other side, and provides a measure of how well the neural response discriminates between the two attention conditions. A KS distance of 0 indicates identical firing rate distributions between attention conditions, while a value of 1 implies complete separation between them.

Linear decoding

We employed linear decoders to quantify the amount of information about either the physical stimulus presented (e.g. the object at the attended location) or the locus of spatial attention in the recorded populations of neurons on a trial-by-trial basis. Linear decoders have been previously shown to reliably extract multidimensional information encoded by neuronal ensembles[8,56,57]. We performed this analysis separately for each recording session using every recorded stable site to prevent bias towards any category. To quantify neural information in a time-resolved manner, firing rates were calculated in 150 ms bins with a sliding window of 10 ms. For each time bin, we trained a logistic regression classifier with L1 regularization and C = 0.1, implemented using the scikit-learn library. To address class imbalance, we adjusted the logistic regression loss function weights inversely proportional to class frequencies in the input data. Multiclass problems were handled using a "one-vs-rest" approach, where a separate binary classifier was trained for each class against the remaining ones. At test time, a sample (population response in a time bin) was classified according to the model with the highest probability output.

To evaluate the decoding performance, we used classification accuracy. Accuracy was estimated using a 10-fold exemplar-grouped cross-validation approach. In each validation step, we split the trials so that each repetition of a particular image could be in either the training or the test set, with each image exemplar being tested at least once. Before classification, net spike counts were z-standardized to ensure that classification was not influenced by the absolute magnitude of the responses. Training and test sets were not scaled independently but the same scaling was applied to both. Chance-level decoding performance was determined by shuffling trial indices 250 times per time window. Observed decoding accuracy was compared against this null distribution using a one-sided permutation test, and only clusters of 5 or more consecutive significant bins were considered.

Cross-condition generalization

We implemented a cross-condition decoding analysis where linear decoders were trained on trials belonging to one attentional condition and tested on trials from a different condition. This approach was applied to examine two distinct aspects. First, when decoding physical stimulus information, decoders were trained on trials where attention was directed to one location and tested on trials where attention was directed to the opposite location. This enabled us to investigate how object representations are modulated when spatial attention changes. Secondly, when decoding the locus of attention, decoders were trained on trials where attention was cued to one object category (e.g., hands) and tested on trials

with the other cued category (e.g., legs). This strategy helped ensure that observed attentional effects were genuinely driven by shifts in spatial attention and not by any incidental differences in the representation of the cued objects themselves.

In both cases the held-out images belonged to the same object exemplars for training and test conditions. To assess significance for the decoding performance of the generalization sets, we performed permutation tests where the null distribution was created by shuffling the labels of both the training set and the generalization test set.

Cross-temporal decoding

To investigate the temporal dynamics of population activity, we performed a cross-temporal decoding analysis. Linear decoders were trained on data from one time period and tested on data from a different time period. This approach was extended to our cross-condition generalization paradigm to whether the dynamics of the decoded information generalized across conditions. Decoding accuracies along the diagonal (e.g. Figures 5C & 6D) represent performance when the classifier is trained and tested on the same time bin. Spike counts were calculated within 150 ms windows, advanced in 10 ms steps, consistent with our standard decoding analysis.

Declarations

Competing interests

The authors declare no competing interests.

Funding

This work was supported by Fonds Wetenschappelijk Onderzoek (FWO) grant G0B6422N and KU Leuven grant C14/22/134. T.T. is Senior Clinical Investigator of FWO Flanders (FWO 1830722N). T.T. holds a Medtronic learning chair. M.V. holds an FWO fellowship for fundamental research (1169321N).

Author Contribution

J.G.R. conceived and designed the experiments. T.T. and M.V. planned and performed array implantations. M.V. performed the recordings. M.V. performed all clinical trial-related activities. J.G.R. performed the data analysis. M.V. and J.G.R. wrote the manuscript. T.T. and P.J. supervised and guided the study. All authors reviewed and edited the manuscript.

Acknowledgement

We are grateful to both patients for their participation. We thank Stijn Verstraeten and Wouter Depuydt for technical assistance with the recording setup, Anaïs Van Hoylandt for assisting with data recording and data monitoring and Thomas Decramer for fine-tuning the implantation and recording technique from Utah-arrays in humans.

Data Availability

The raw data is uploaded to a figshare repository at https://doi.org/10.6084/m9.figshare.32293278.

References

1. Posner, M. I. Orienting of attention. *Q. J. Exp. Psychol.* **32**, 3–25. https://doi.org/10.1080/00335558008248231 (1980).
2. Treisman, A. M. & Gelade, G. A feature-integration theory of attention. *Cogn. Psychol.* **12**, 97–136. https://doi.org/10.1016/0010-0285(80)90005-5 (1980).
3. Mitchell, J. F., Sundberg, K. A. & Reynolds, J. H. Differential attention-dependent response modulation across cell classes in macaque visual area V4. *Neuron* 55, 131–141 (2007). https://doi.org/10.1016/j.neuron.2007.06.018
4. Mitchell, J. F., Sundberg, K. A. & Reynolds, J. H. Spatial attention decorrelates intrinsic activity fluctuations in macaque area V4. *Neuron* 63, 879–888 (2009). https://doi.org/10.1016/j.neuron.2009.09.013
5. Sundberg, K. A., Mitchell, J. F. & Reynolds, J. H. Spatial attention modulates center-surround interactions in macaque visual area v4. *Neuron* 61, 952–963 (2009). https://doi.org/10.1016/j.neuron.2009.02.023
6. Treue, S. & Maunsell, J. H. Attentional modulation of visual motion processing in cortical areas MT and MST. *Nature* **382**, 539–541. https://doi.org/10.1038/382539a0 (1996).
7. Reynolds, J. H., Chelazzi, L. & Desimone, R. Competitive mechanisms subserve attention in macaque areas V2 and V4. *J. Neurosci.* **19**, 1736–1753. https://doi.org/10.1523/JNEUROSCI.19-05-01736.1999 (1999).
8. Tremblay, S., Pieper, F., Sachs, A. & Martinez-Trujillo, J. Attentional filtering of visual information by neuronal ensembles in the primate lateral prefrontal cortex. *Neuron* **85**, 202–215. https://doi.org/10.1016/j.neuron.2014.11.021 (2015).
9. Ghose, G. M. & Maunsell, J. H. Spatial summation can explain the attentional modulation of neuronal responses to multiple stimuli in area V4. *J. Neurosci.* **28**, 5115–5126. https://doi.org/10.1523/JNEUROSCI.0138-08.2008 (2008).
10. Zhang, Y. et al. Object decoding with attention in inferior temporal cortex. *Proc. Natl. Acad. Sci. U S A*. **108**, 8850–8855. https://doi.org/10.1073/pnas.1100999108 (2011).

11. Buschman, T. J. & Kastner, S. From Behavior to Neural Dynamics: An Integrated Theory of Attention. *Neuron* 88, 127–144 (2015). https://doi.org/10.1016/j.neuron.2015.09.017
12. Miller, E. K. & Buschman, T. J. Cortical circuits for the control of attention. *Curr. Opin. Neurobiol.* **23**, 216–222. https://doi.org/10.1016/j.conb.2012.11.011 (2013).
13. McAdams, C. J. & Maunsell, J. H. Effects of attention on the reliability of individual neurons in monkey visual cortex. *Neuron* **23**, 765–773. https://doi.org/10.1016/s0896-6273(01)80034-9 (1999).
14. Fries, P., Reynolds, J. H., Rorie, A. E. & Desimone, R. Modulation of oscillatory neuronal synchronization by selective visual attention. *Science* **291**, 1560–1563. https://doi.org/10.1126/science.1055465 (2001).
15. Moran, J. & Desimone, R. Selective attention gates visual processing in the extrastriate cortex. *Science* **229**, 782–784. https://doi.org/10.1126/science.4023713 (1985).
16. Cohen, M. R. & Maunsell, J. H. Attention improves performance primarily by reducing interneuronal correlations. *Nat. Neurosci.* **12**, 1594–1600. https://doi.org/10.1038/nn.2439 (2009).
17. Motter, B. C. Focal attention produces spatially selective processing in visual cortical areas V1, V2, and V4 in the presence of competing stimuli. *J. Neurophysiol.* **70**, 909–919. https://doi.org/10.1152/jn.1993.70.3.909 (1993).
18. Desimone, R. & Schein, S. J. Visual properties of neurons in area V4 of the macaque: sensitivity to stimulus form. *J. Neurophysiol.* **57**, 835–868. https://doi.org/10.1152/jn.1987.57.3.835 (1987).
19. Cavanaugh, J. R., Bair, W. & Movshon, J. A. Nature and interaction of signals from the receptive field center and surround in macaque V1 neurons. *J. Neurophysiol.* **88**, 2530–2546. https://doi.org/10.1152/jn.00692.2001 (2002).
20. Desimone, R. & Duncan, J. Neural mechanisms of selective visual attention. *Annu. Rev. Neurosci.* **18**, 193–222. https://doi.org/10.1146/annurev.ne.18.030195.001205 (1995).
21. Ruff, D. A., Ni, A. M. & Cohen, M. R. Cognition as a Window into Neuronal Population Space. *Annu. Rev. Neurosci.* **41**, 77–97. https://doi.org/10.1146/annurev-neuro-080317-061936 (2018).
22. Heinze, H. J. et al. Combined spatial and temporal imaging of brain activity during visual selective attention in humans. *Nature* **372**, 543–546. https://doi.org/10.1038/372543a0 (1994).
23. Vandenberghe, R. et al. Attention to one or two features in left or right visual field: a positron emission tomography study. *J. Neurosci.* **17**, 3739–3750. https://doi.org/10.1523/JNEUROSCI.17-10-03739.1997 (1997).
24. Kastner, S., De Weerd, P., Desimone, R. & Ungerleider, L. G. Mechanisms of directed attention in the human extrastriate cortex as revealed by functional MRI. *Science* **282**, 108–111. https://doi.org/10.1126/science.282.5386.108 (1998).
25. Malach, R. et al. Object-related activity revealed by functional magnetic resonance imaging in human occipital cortex. *Proc. Natl. Acad. Sci. U S A*. **92**, 8135–8139. https://doi.org/10.1073/pnas.92.18.8135 (1995).

26. Grill-Spector, K.et al. A sequence of object-processing stages revealed by fMRI in the human occipital lobe.*Hum Brain Mapp* 6, 316–328 (1998). https://doi.org/10.1002/(SICI)1097-0193(1998)6:4<316::AID-HBM9>3.0.CO;2-6
27. Decramer, T. et al. Single-cell selectivity and functional architecture of human lateral occipital complex. *PLoS Biol.* **17**, e3000280. https://doi.org/10.1371/journal.pbio.3000280 (2019).
28. Grill-Spector, K. K. & Kanwisher, Z. The lateral occipital complex and its role in object recognition. *Vis. Res.* **41**, 1409–1422 (2001).
29. Vanhoyland, M., Janssen, P. & Theys, T. Single-neuron correlates of visual consciousness in human lateral occipital complex. *Nat. Commun.* **16**, 11008. https://doi.org/10.1038/s41467-025-67077-w (2025).
30. Bougou, V. et al. Neuronal tuning and population representations of shape and category in human visual cortex. *Nat. Commun.* **15**, 4608. https://doi.org/10.1038/s41467-024-49078-3 (2024).
31. Ito, M. & Gilbert, C. D. Attention modulates contextual influences in the primary visual cortex of alert monkeys. *Neuron* **22**, 593–604. https://doi.org/10.1016/s0896-6273(00)80713-8 (1999).
32. Mountcastle, V. B., Motter, B. C., Steinmetz, M. A. & Sestokas, A. K. Common and differential effects of attentive fixation on the excitability of parietal and prestriate (V4) cortical visual neurons in the macaque monkey. *J. Neurosci.* **7**, 2239–2255. https://doi.org/10.1523/JNEUROSCI.07-07-02239.1987 (1987).
33. Roelfsema, P. R. & Spekreijse, H. The representation of erroneously perceived stimuli in the primary visual cortex. *Neuron* **31**, 853–863. https://doi.org/10.1016/s0896-6273(01)00408-1 (2001).
34. Spitzer, H., Desimone, R. & Moran, J. Increased attention enhances both behavioral and neuronal performance. *Science* **240**, 338–340. https://doi.org/10.1126/science.3353728 (1988).
35. Reynolds, J. H. & Heeger, D. J. The normalization model of attention. *Neuron* **61**, 168–185. https://doi.org/10.1016/j.neuron.2009.01.002 (2009).
36. Chelazzi, L., Miller, E. K., Duncan, J. & Desimone, R. A neural basis for visual search in inferior temporal cortex. *Nature* **363**, 345–347. https://doi.org/10.1038/363345a0 (1993).
37. Curtis, C. E. & D'Esposito, M. Persistent activity in the prefrontal cortex during working memory. *Trends Cogn. Sci.* **7**, 415–423. https://doi.org/10.1016/s1364-6613(03)00197-9 (2003).
38. Postle, B. R. Working memory as an emergent property of the mind and brain. *Neuroscience* **139**, 23–38. https://doi.org/10.1016/j.neuroscience.2005.06.005 (2006).
39. Wolfe, J. M., Vo, M. L., Evans, K. K. & Greene, M. R. Visual search in scenes involves selective and nonselective pathways. *Trends Cogn. Sci.* **15**, 77–84. https://doi.org/10.1016/j.tics.2010.12.001 (2011).
40. Luria, R., Balaban, H., Awh, E. & Vogel, E. K. The contralateral delay activity as a neural measure of visual working memory. *Neurosci. Biobehav Rev.* **62**, 100–108. https://doi.org/10.1016/j.neubiorev.2016.01.003 (2016).

41. Awh, E., Vogel, E. K. & Oh, S. H. Interactions between attention and working memory. *Neuroscience* **139**, 201–208. https://doi.org/10.1016/j.neuroscience.2005.08.023 (2006).
42. Vanhoyland, M., Janssen, P. & Theys, T. Human lateral occipital complex is invariant for position and size transformations at the single-neuron level. *Sci. Rep-Uk*. https://doi.org/10.1038/s41598-026-43946-2 (2026).
43. Jeanne, J. M., Sharpee, T. O. & Gentner, T. Q. Associative learning enhances population coding by inverting interneuronal correlation patterns. *Neuron* **78**, 352–363. https://doi.org/10.1016/j.neuron.2013.02.023 (2013).
44. Ruff, D. A. & Cohen, M. R. Attention can either increase or decrease spike count correlations in visual cortex. *Nat. Neurosci.* **17**, 1591–1597. https://doi.org/10.1038/nn.3835 (2014).
45. Verhoef, B. E. & Maunsell, J. H. R. Attention-related changes in correlated neuronal activity arise from normalization mechanisms. *Nat. Neurosci.* **20**, 969–977. https://doi.org/10.1038/nn.4572 (2017).
46. Ramirez, J. G. et al. Intracortical recordings reveal the neuronal selectivity for bodies and body parts in the human visual cortex. *Proc. Natl. Acad. Sci. U S A*. **121**, e2408871121. https://doi.org/10.1073/pnas.2408871121 (2024).
47. Decramer, T. et al. Single-Unit Recordings Reveal the Selectivity of a Human Face Area. *J. Neurosci.* **41**, 9340–9349. https://doi.org/10.1523/JNEUROSCI.0349-21.2021 (2021).
48. Martinet, L. E. et al. Human seizures couple across spatial scales through travelling wave dynamics. *Nat. Commun.* **8**, 14896. https://doi.org/10.1038/ncomms14896 (2017).
49. Smith, E. H. et al. The ictal wavefront is the spatiotemporal source of discharges during spontaneous human seizures. *Nat. Commun.* **7**, 11098. https://doi.org/10.1038/ncomms11098 (2016).
50. Truccolo, W. et al. Single-neuron dynamics in human focal epilepsy. *Nat. Neurosci.* **14**, 635–641. https://doi.org/10.1038/nn.2782 (2011).
51. Bougou, V. et al. Mesoscale insights in Epileptic Networks: A Multimodal Intracranial Dataset. *Sci. Data*. **12**, 774. https://doi.org/10.1038/s41597-025-05026-4 (2025).
52. Fonov, V. et al. Unbiased average age-appropriate atlases for pediatric studies. *Neuroimage* **54**, 313–327. https://doi.org/10.1016/j.neuroimage.2010.07.033 (2011).
53. Blenkmann, A. O. et al. iElectrodes: A Comprehensive Open-Source Toolbox for Depth and Subdural Grid Electrode Localization. *Front. Neuroinform*. **11**, 14. https://doi.org/10.3389/fninf.2017.00014 (2017).
54. Bracci, S. & de Op, H. Dissociations and Associations between Shape and Category Representations in the Two Visual Pathways. *J. Neurosci.* **36**, 432–444. https://doi.org/10.1523/JNEUROSCI.2314-15.2016 (2016).
55. Popivanov, I. D., Jastorff, J., Vanduffel, W. & Vogels, R. Stimulus representations in body-selective regions of the macaque cortex assessed with event-related fMRI. *Neuroimage* **63**, 723–741. https://doi.org/10.1016/j.neuroimage.2012.07.013 (2012).

56. Astrand, E., Wardak, C. & Ben Hamed, S. Selective visual attention to drive cognitive brain-machine interfaces: from concepts to neurofeedback and rehabilitation applications. *Front. Syst. Neurosci.* **8**, 144. https://doi.org/10.3389/fnsys.2014.00144 (2014).

57. Rigotti, M. et al. The importance of mixed selectivity in complex cognitive tasks. *Nature* **497**, 585–590. https://doi.org/10.1038/nature12160 (2013).

58. Vanhoyland, M., Janssen, P. & Theys, T. Data from Intracortical recordings in human lateral occipital complex support the biased-competition model of spatial attention *FigShare* (2026). https://doi.org/10.6084/m9.figshare.32293278

Figures

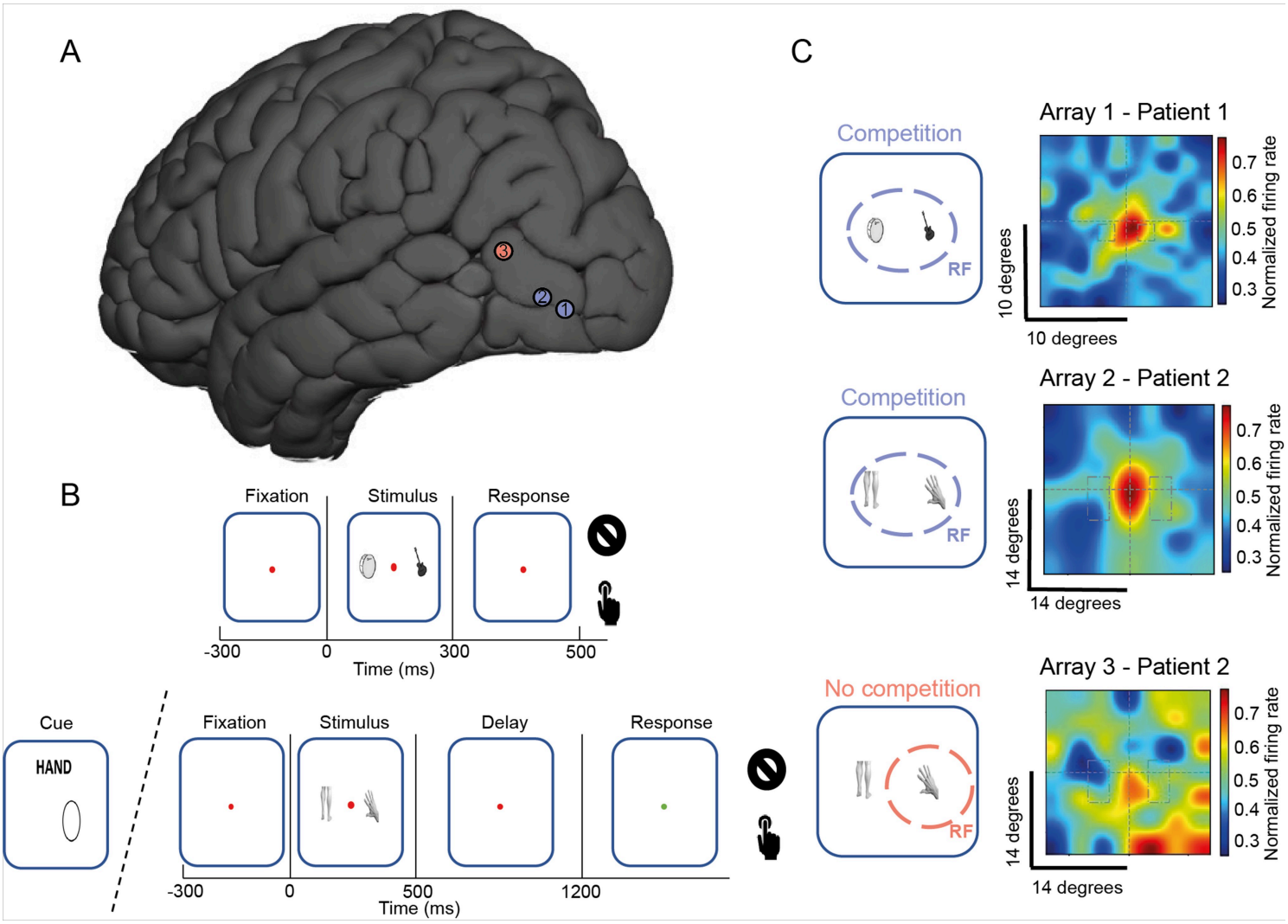


Figure 1

Recording sites, task description and receptive fields.

(A) Anatomical locations of Utah arrays projected on a common MNI template of the brain. MNI coordinates (X, Y, Z) are as follows: A1 (-35, -89, -8), A2 (-41, -83, 9) and A3 (-38, -84, -5). Blue arrays

represent competition arrays, red represents non-competition array. Array 2 and 3 were implanted in the same patient (P2). Adapted from Bougou, V., Vanhoyland, M., Bertrand, A. et al. Neuronal tuning and population representations of shape and category in human visual cortex. Nat Commun 15, 4608 (2024).[30] **(B)** Schematic of the spatial attention tasks. Patients were instructed to press a button if they witnessed the cued object in the correct location. Above, scheme for P1: Trials began with central fixation (200-300 ms), followed by the simultaneous presentation of two object images. A verbal cue at the start of each block indicated the target object and the side of the screen where the target would trigger a button press response. After stimulus presentation (300 ms), the patient responded via button press. Below, scheme for P2: A visual cue (3000 ms) at block start indicated the target object and location. Trials involved central fixation (200-300 ms), followed by two object images (500 ms). After a blank screen delay (700 ms), the fixation marker changed color, signaling the response period. **(C) Left**. Electrode array configurations with respect to stimulus presentation. In competition arrays (A1 and A2, blue) the average RF encompassing both object presentation locations. In contrast, only the right location was within the average RF of the no-competition array (A3, red). **Right.** Heatmap showing the population average RF per recorded array. Overlayed dashed boxes correspond to both objects' presentation locations.

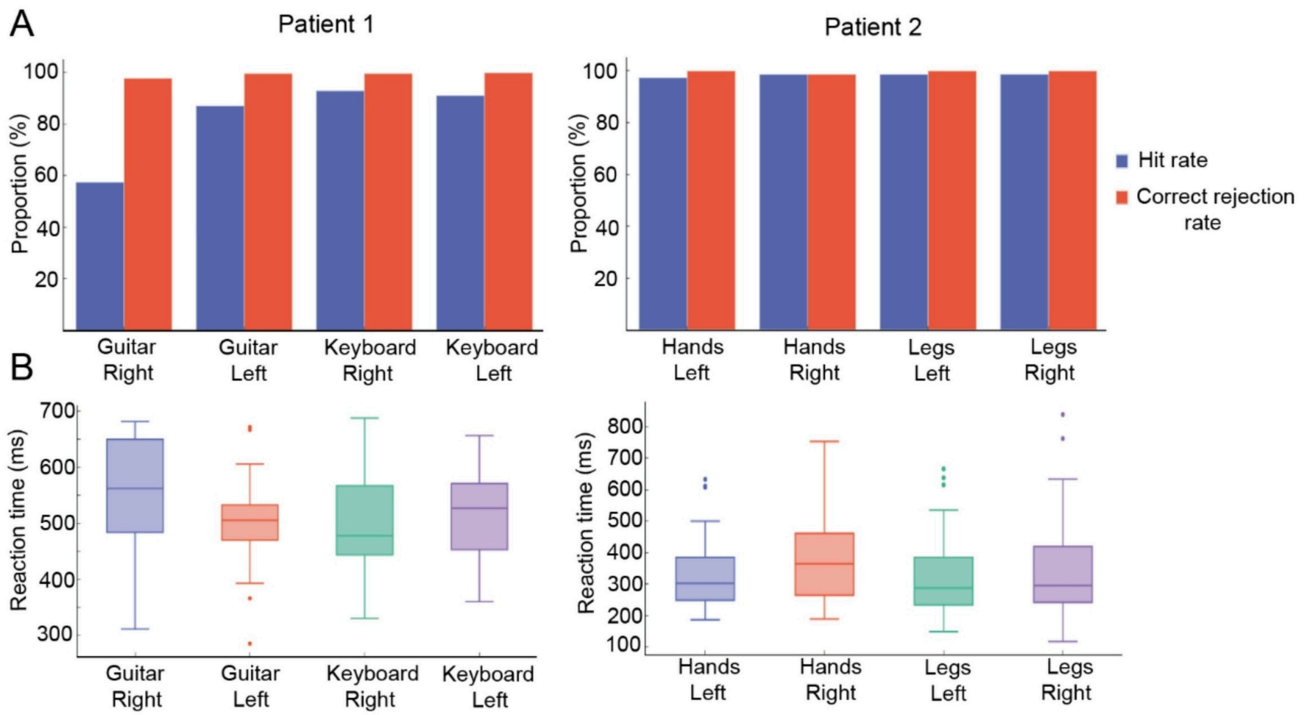


Figure 2

Behavioral performance.

(A) Proportion of correct responses (Hit Rate, blue bars) and correct rejections (Correct Rejection Rate, orange bars) for each cue condition for P1 (Left) and P2 (Right). Hit Rate refers to the proportion of trials where the patient correctly responded to the cued target. Correct Rejection Rate refers to the proportion of trials where the patient withheld a response when no target was present**. (B)** Box plots showing the reaction times (ms) for correct detections across cue conditions for P1 (Left) and P2 (Right). Box plots indicate median (middle line), 25th, 75th percentile (box), and box limits ± 1.5 × interquartile range (whiskers).

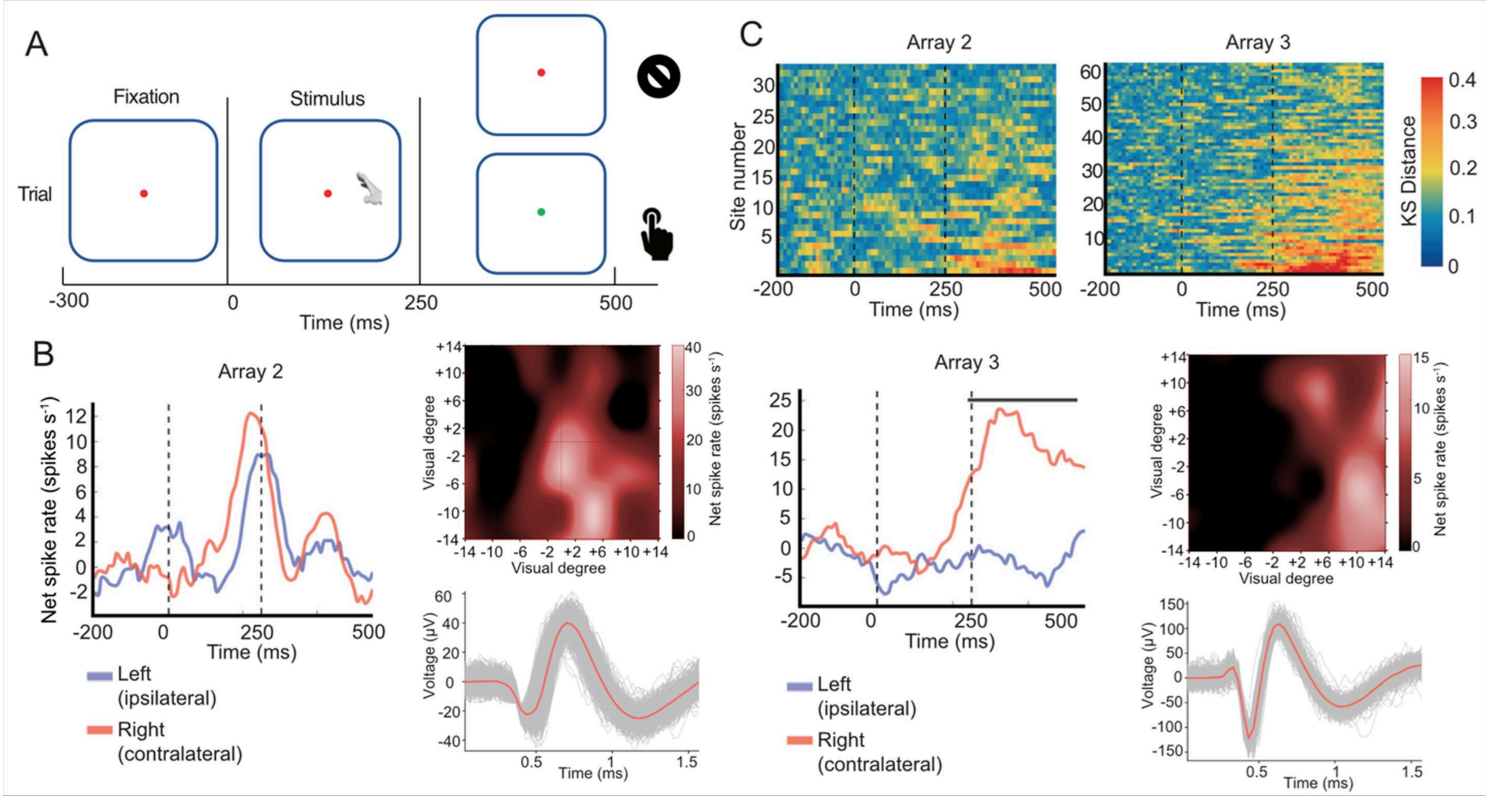


Figure 3

Control task in P2.

(A) Schematic of the attention control task that was performed in array 2 and 3. The patient had to press a button if she noticed a change in the color of the fixation marker. Each trial began with central fixation (200-300 ms), followed by the presentation of an individual object from the attention task stimulus set at one of both task locations. After stimulus presentation (300 ms), the patient responded via button press. **(B)** Example single units per array. Average net spike rate for trials where the object was presented at the ipsilateral location (left, blue) and contralateral location (right, red). Horizontal black lines indicate time windows with statistically significant differences between left and right trials (two-sided independent samples t-test, $p < 0.01$). At the right side of each graph, the waveform and receptive field is presented (time window 100 - 250 and 200 - 350 ms after stimulus onset was used for array 2 and 3, respectively). **(C)** Kolmogorov-Smirnov (KS) distances across time. Each row illustrates the KS distance of a visually responsive site between distribution of trials with objects presented at the left versus trials with objects

presented to the right. Time bins are shown on the x-axis and values represent the middle of a 100 ms bin. Sites are sorted in ascending order from top to bottom according to the maximum KS distance.

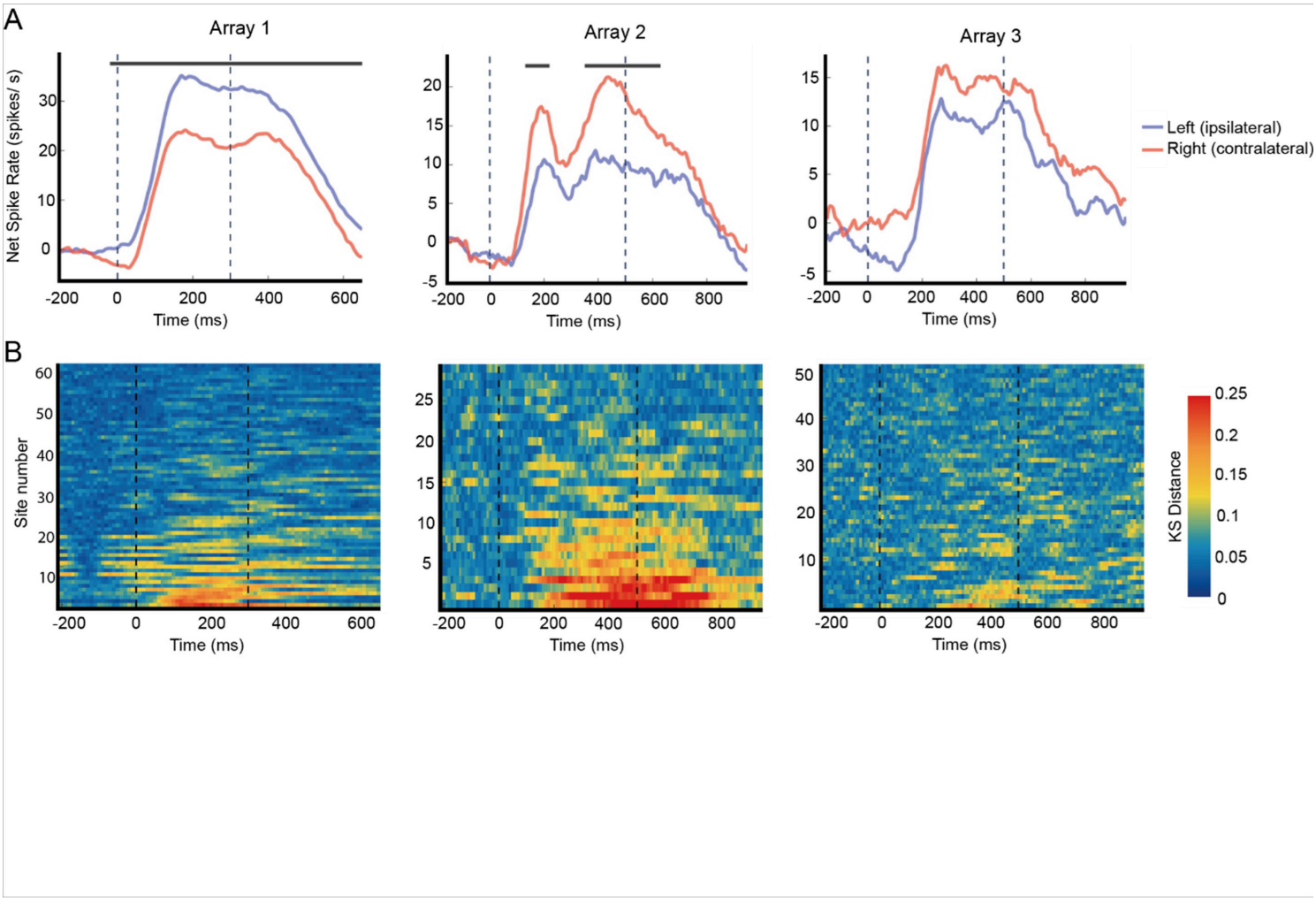


Figure 4

Spatial attention modulations for individual sites.

(A) Average net spike rate for trials attending left (blue) and right (red) across example sites from each recording array. Horizontal black lines indicate time windows with statistically significant differences between left and right trials (two-sided independent samples t-test, $p < 0.05$). **(B)** Kolmogorov-Smirnov (KS) distances across time. Each row illustrates the KS distance of a visually responsive site between distribution of trials attending to the left versus trials attending to the right. Time bins are shown on the x-axis and values represent the middle of a 100 ms bin. Sites are sorted in ascending order from top to bottom according to the maximum KS distance.

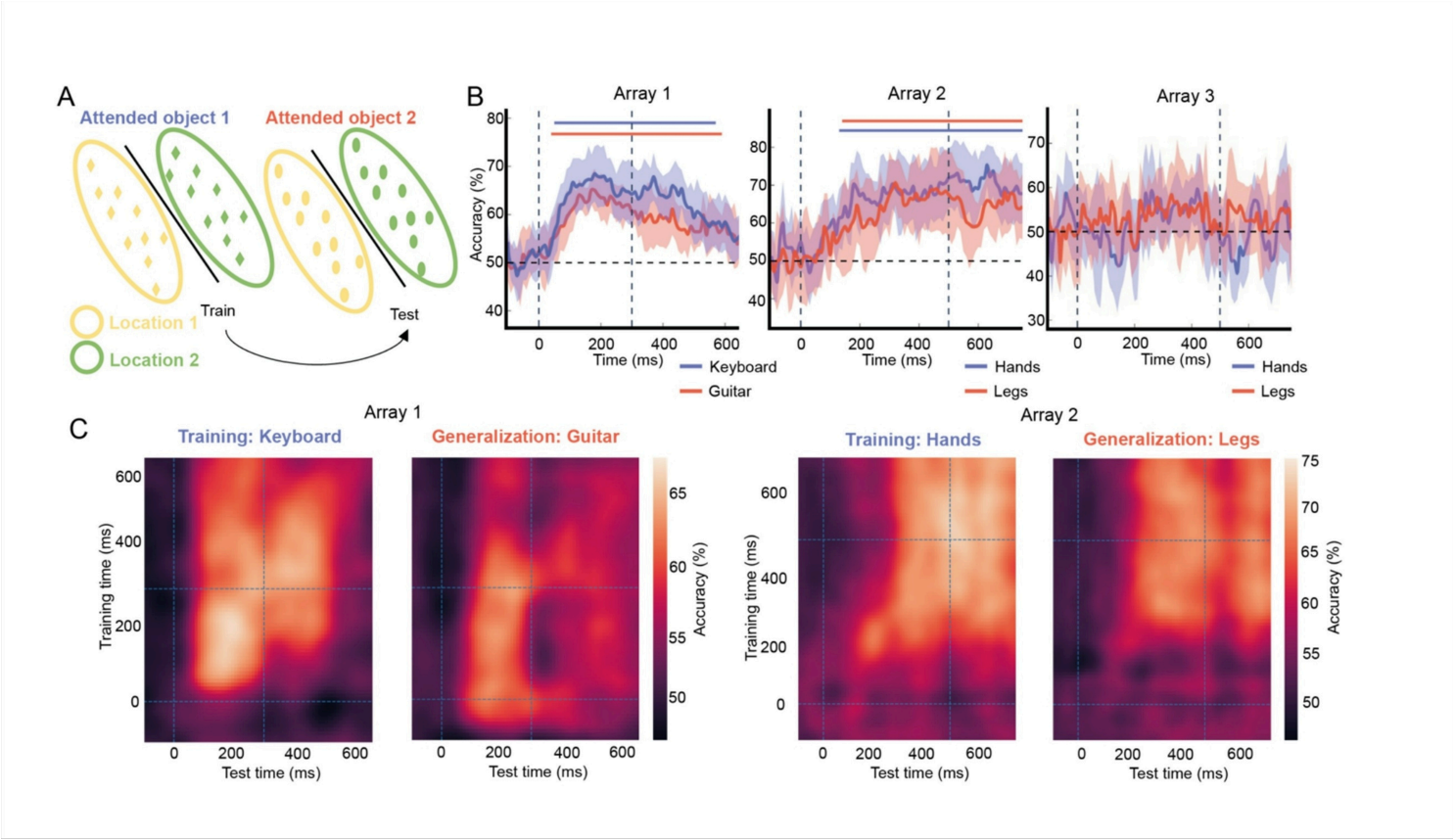


Figure 5

Decoding locus of spatial attention.

(A) Schematic of the cross-condition generalization procedure for decoding the locus of spatial attention. Linear decoders were trained to discriminate between trials attending to left (ipsilateral, yellow) versus right (contralateral, green) using one target object (Keyboard and Hands for P1 and P2, respectively) and tested on generalization data of trials with the other target object (Guitar and Legs for P1 and P2, respectively). **(B)** Time course of decoder performance (Accuracy) for predicting the locus of attention regardless of the stimulus in the competition (A1 and A2, green) and no competition (A3, blue) conditions. Lines and shading show mean ± standard error classification accuracy for (blue) decoders trained to discriminate between the attended locations using trials with one target object and tested using held-out data from the same target object. Red curves correspond to cross-condition generalization performance, where the decoder is tested using data from a different target object. Distribution reflects 10-fold grouped cross-validation. Horizontal bars indicate above-chance classification ($p < 0.005$; one-sided permutation test with at least five consecutive significant time points). **(C)** Temporal dynamics of spatial attention effects. Cross-time decoding analysis for competition arrays (A1 and A2) for trials with the training target object (same as in Fig 5B) and for the trials for the generalization object. Color scale represents decoding accuracies for linear decoders trained to predict the locus of attention. Training time of the decoder is shown on the y-axis and test time is shown on the x-axis. Dashed blue lines represent times of stimulus onset and offset. Note the drop in

accuracy after the second blue-dashed line in the generalization analysis of A1. In **(B-D)**, time bins on x-axis **(B-C)** and x- and y-axis **(D)**represent the middle of a 150 ms bin used for decoding.

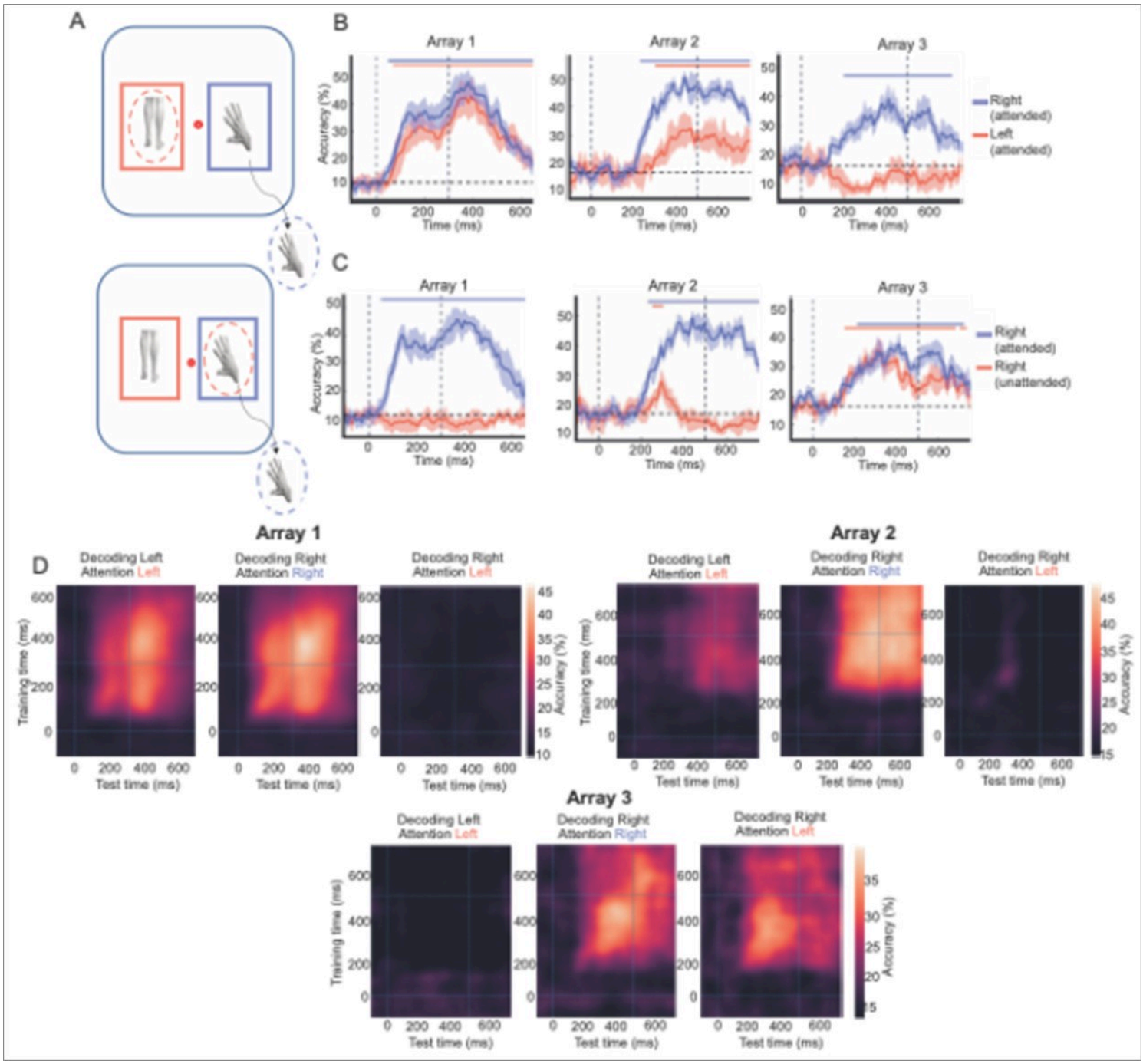


Figure 6

Decoding object at attended location or fixed location.

(A) Schematic of the procedure for decoding the object at the attended location (above) and fixed location (below). In both procedures, the decoder was first trained on trials attending to the right (blue square) to predict the attended object at the right (blue circle) and then tested for generalization on trials where attention was directed to the other location (red square). The red circle shows where an object

was predicted during testing for generalization. Therefore, the generalization for attended location analysis investigated if an object was decodable at an attended location while being trained at another, but also attended, location. The generalization for fixed location analysis investigated if an object was decodable at an unattended location while being trained at the same, but attended, location. **(B)** Time course of decoder performance (accuracy) for each recording session. Lines and shading show mean ± 1std classification accuracy for (blue) decoders trained to decode the object at the attended location when the decoder is trained and tested at the same location and (red) decoders trained at one location and tested on the other. Distribution reflects 10-fold grouped cross-validation. Horizontal bars indicate above-chance classification ($p < 0.005$; one-sided permutation test with at least five consecutive significant time points). **(C)** Time course of decoder performance for each recording session. Lines and shading show mean ± 1std classification accuracy for (Blue) decoders trained to decode the object at a fixed location when the decoder is trained and tested at the same location and (Red) decoders trained at one fixed location and tested on the other. Distribution reflects 10-fold grouped cross-validation. Horizontal bars indicate above-chance classification ($p < 0.005$; one-sided permutation test with at least five consecutive significant time points). **(D)** Cross-time decoding analysis for neural decoders trained to predict the stimulus at different locations for every recorded array (upper plots are competition arrays, lower plots are from the non-competition array). For each array, central matrices present cross-time decoding analysis for the training case, where decoders were trained to predict the stimulus located at the right when attention is directed to the right. In contrast, the left and right matrices display cross-time decoding performance in the generalization cases, where the training decoder is tested to predict the stimulus at either the right or left locations when attention was directed to the left. Decoding accuracies for linear decoders trained on attended locations are color-coded. Training time is plotted on the y-axis, and test time on the x-axis. Dashed blue lines indicate stimulus onset and offset. In **(B, C and D)**, time bins on x-axis (**B,C**) and x- and y-axis (**D**) represent the middle of a 150 ms bin used for decoding.